Tianyi Guo[1,2]
Yin Wei[3]
Changqing Xu[3]
Benjamin R. Watts[3]
Zhiyi Zhang[4]
Qiyin Fang[1,3]
Haiying Zhang[2]
P. Ravi Selvaganapathy[5]
M. Jamal Deen[1,6]

[1]School of Biomedical Engineering, McMaster University, Hamilton, Canada
[2]Institute of Microelectronics, Chinese Academy of Science, Beijing, China
[3]Department of Engineering Physics, McMaster University, Hamilton, Canada
[4]Information and Communication Technologies, National Research Council of Canada, Ottawa, Canada
[5]Department of Mechanical Engineering, McMaster University, Hamilton, Canada
[6]Department of Electrical and Computer Engineering, McMaster University, Hamilton, Canada

Research Article

Counting of *Escherichia coli* by a microflow cytometer based on a photonic–microfluidic integrated device

Counting of *Escherichia coli* DH5α-cell suspensions in PBS is performed using a microflow cytometer based on a photonic–microfluidic integrated device. Side-scattered light signals are used to count the *E. coli* cells. A detection efficiency of 92% is achieved when compared with the expected count from a hemocytometer. The detection efficiency is correlated to the ratio of sample to sheath flow rates. It is demonstrated that *E. coli* can be easily distinguished from beads of similar sizes (2–4 μm) as their scattering intensities are different.

1 Introduction

The presence of coliforms in drinking water is considered as a possible indicator of pathogenic bacteria that can cause waterborne diseases or even fatalities. Generally, *Escherichia coli* is selected to be an indicator of the microbiological parameter of water quality [1]. Existing methods such as the membrane filter technique involving bacterial culture are time-consuming to detect total coliforms or *E. coli* [2]. In addition, only a small percentage (<3%) of the total bacterial population present in environmental water is culturable, which further limits the use of culture-based methods to detect bacteria [3]. Thus, current methods do not provide real-time or accurate information on the presence or absence of bacteria in water so that timely actions to prevent the spread of waterborne diseases can be taken if bacteria are present. For example, the total number of waterborne illnesses per year in the United States has been estimated at 19.5 million with 17% associated

to bacteria in drinking water [4]. Therefore, there is a critical need for simple and rapid detection of bacteria in the water-distribution network.

Many techniques have been proposed to rapidly detect bacteria. They include enzymatic methods, immunological methods, PCR methods and in situ hybridization techniques [1, 5]. Many of these methods require sample preparation that cannot be performed on site or require expensive reagents. Flow cytometry has been used for rapid detection of pathogenic *E. coli* [6, 7], enumeration of total bacteria [8–12], assessment of bacterial viability [13], and determination of bacterial growth phase [14] but with staining of the cells or their constituents with fluorescent tags. Although this approach increases the speed of detection, it still uses expensive flow cytometers and additional sample preparation steps that limit their on-site use [15].

Microflow cytometers based on micro-fabricated fluidic devices provide considerable opportunities to overcome the limitation of high operating cost because the amount of reagents needed by a microfluidic device is dramatically reduced [16]. Furthermore, integration of optical components such as waveguides, buried fibers, or lenses [17] into the microfluidic devices replaces the bulk lens system and aligns optical paths automatically, thus increasing portability, shock

Abbreviations: PMT, photo multiplier tube; **SSC**, side scattered

resistance, and reliability [18–21]. Compared with conventional flow cytometers that utilize 3D hydrodynamic sample centering and 3D light focusing in free space to ensure good interaction between excitation light beam and interrogated particles, most microflow cytometers suffer from the planar structures that only allow for 2D sample centering and 2D light focusing, resulting in a reduced detection efficiency of the particles or cells.

Using 3D optics in free space for excitation light focusing, but 2D sample centering in microfluidic channels by electrokinetics, a detection efficiency of 98% for 0.93 μm fluorescently labeled beads and 94% for *E. coli* labeled with a fluorescein-conjugated antibody at low throughputs was achieved [16, 22]. Using 2D sample centering by hydrodynamics, detection efficiencies <89% for both 1 μm fluorescently labeled beads and *E. coli* were resolved [23]. Further improvements using a 3D sample centering by a multichannel hydrodynamic focusing led to a detection efficiency of 97% for fluorescent latex beads [24].

Although the performance of microflow cytometers mentioned above was good, they rely on bulk optical lens system for beam shaping. To reduce the system complexity and cost, a microflow cytometer based on a photonic–microfluidic integrated device was developed [25–27]. This system eliminated the bulk optical lens system for beam shaping and integrated the input and output waveguides, beam-shaping lens system, and microfluidic channels in one chip. Its performance was evaluated with tests using polystyrene beads of different sizes, demonstrating comparable CVs to conventional flow cytometers [28].

In this work, we present the counting of *E. coli* DH5α-cell suspensions in PBS solution using the microflow cytometer based on the photonic–microfluidic integrated device, which only utilizes on-chip lens system for 2D light focusing and 2D hydrodynamic sample centering. Side-scattered (SSC) light signals are collected in free space and used to count *E. coli* without tagging the cells. This microflow cytometer allows for separation of the bacteria from noise due to particles of similar sizes.

This article is organized as follows. In Section 2, we describe the system design and experiments, including the photonic–microfluidic integrated device, system setup, sample preparation, data collection, and analysis. In Section 3, we present and discuss the results, highlighting the system performance through testing with microbeads, counting *E. coli* and separation of *E. coli* from background noise due to similar-sized particles. Then, to put our work in perspective, we tabulate the key performance measures of similar microflow cytometers and ours. Finally, the conclusions are given in Section 4.

2 Materials and methods

2.1 Photonic–microfluidic integrated device

The design, structure, and fabrication of the photonic–microfluidic integrated device had been reported in detail in previous publications [25–32]. In Fig. 1, a1 shows a photo of fabricated device and a2 illustrates its 3D model; b1 and b2 show top view and front view of the device model, respectively. The device consists of four layers, pyrex glass substrate, 30-μm-thick SU-8 photoresist layer, PDMS covering layer, and glass pads layer. The SU-8 photoresist layer is lithographically patterned as a functionality layer and sealed by a PDMS covering layer with holes aligned with all inlets and outlet of the functionality layer, forming 50-μm-wide microfluidic channels from sample inlet and sheath flow inlets to the outlet. It also forms optical waveguides with the SU-8 photoresist as core, pyrex glass (bottom), PDMS (top), and air (both sides) as claddings. Glass pads with drilled holes are bonded to PDMS layer and used to fix the inlet and outlet pins. Figure 1c shows a detailed view of the functionality layer in the area indicated by the small rectangle in (b1). Sidewalls of curved patterns where SU-8 photoresist is removed act as a lens system, focusing the light from the input waveguide to the center of microfluidic channel where particles or bacteria will be interrogated, hence this is termed the interrogation region. Two pairs of reflectors are put on both sides of the input light beam to prevent stray light from entering the interrogation region. Such stray light will increase the background noise. Five different lens systems with focused beam widths of 1.5, 3.6, 6, 10, and 12 μm are designed in one device. The one with 10 μm beam size gave the best performance [28], and it is used in all experiments reported here.

The fabrication procedure of this device is optimized to achieve high S/N for weak SSC light detection because the SSC light produced by *E. coli* is much weaker than that by the polystyrene beads of similar sizes due to less refractive index difference between *E. coli* and water. The detection of weak light requires low background noise of the device itself, a main source of which is the scattering of excitation light due to imperfections of the input waveguide, lens system, and microfluidic channels, for example the roughness of these structures. With the optimized device, high S/Ns are achieved for tests on *E. coli*, as detailed in Section 3.

2.2 System setup

The system setup for a microflow cytometer based on the photonic–microfluidic integrated device is shown in Fig. 1d and a photo of the device with input fiber and side-scattering light collection components is shown in Fig. 1e. Light from a 532 nm laser (Beijing Stone Laser, Beijing, China) is coupled into the input waveguide through an optical fiber, then focused to the interrogation region by the on-chip lens system. Beads or bacteria suspensions in a syringe are injected into the sample inlet by a syringe pump and hydrodynamically focused into the center of the microfluidic channel by the sheath flows at both sides. SSC light produced when the samples pass through the interrogation region will be collected by the objective and filtered by an optical filter with a passband of 522–542 nm. A spatial filter with a 1 mm diameter pinhole is used to reject the ambient light. A photomultiplier tube (PMT; Newport, Irvine, CA,
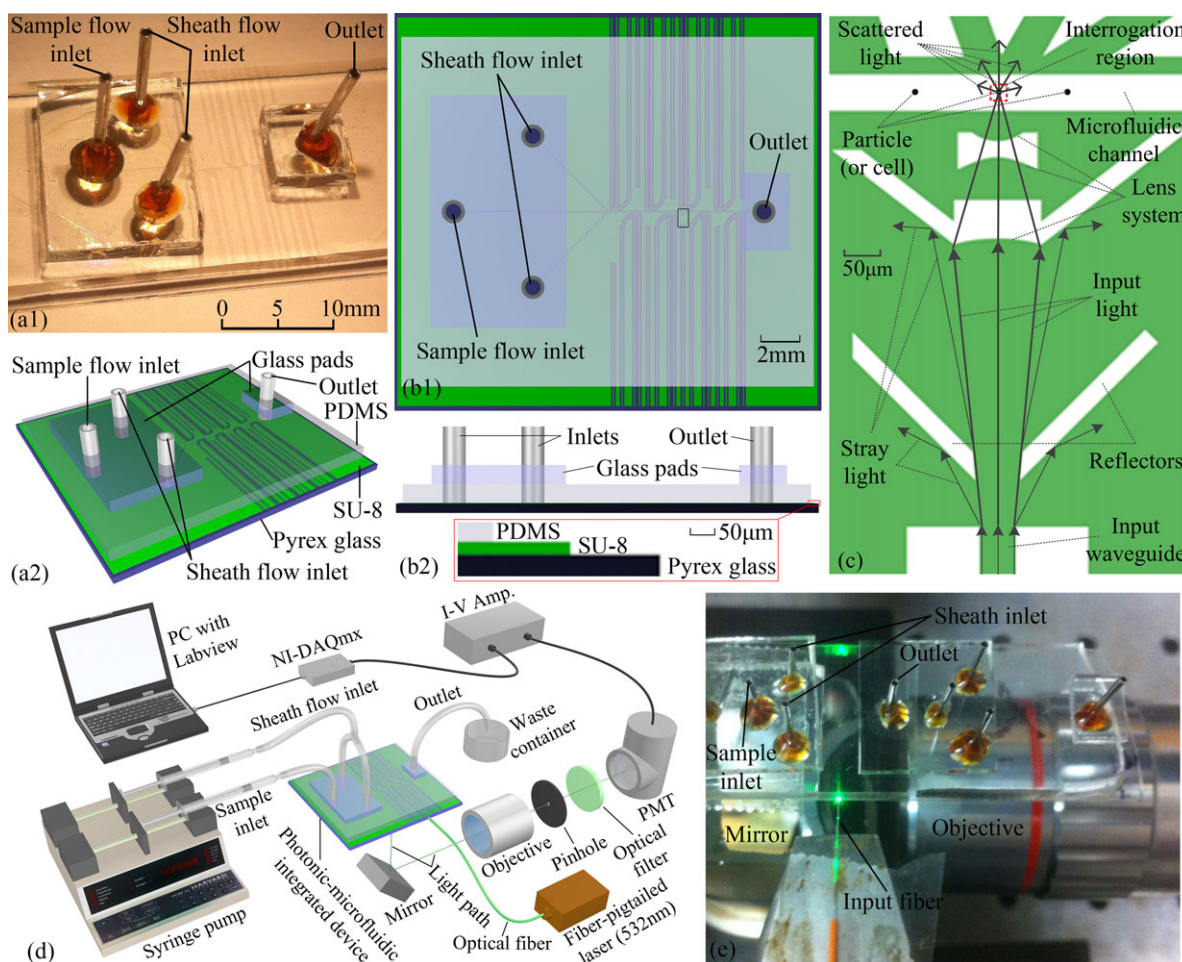
Figure 1. The photonic–microfluidic integrated device, (a1) its photo, (a2) its 3D model, (b1) top view and (b2) front view of the device mode, (c) magnified view of the area indicated by the rectangle in (b1) with light rays (arrows). (d) System setup of a microflow cytometer based on the photonic–microfluidic integrated device; (e) a photo of the device with input fiber and light collection components in the system setup.

USA) is used to detect, convert, and amplify the light signals into current signals, which will be further amplified by a current-to-voltage amplifier to give voltage signals. The voltage signals are then digitized by a data acquisition card (USB-6211, National Instruments, Austin, TX, USA) and recorded by a custom LabView program for data analysis.

The 50-μm-wide microfluidic channel is focused and imaged onto the plane of the 1 mm pinhole through the objective with a lateral magnification of 40 and central alignment between the interrogation region and the pinhole. The pinhole and optical filter are mounted inside the PMT to ensure minimum distance between the pinhole and the photocathode of PMT and complete collection of the scattered light passing through the pinhole. The optical path length between the PMT and the microfluidic channel is about 50 cm.

2.3 Sample preparation

Highly uniform blank polystyrene beads (Invitrogen, Burlington, Canada) with a diameter of 1 μm (1.10 ± 0.04 μm) were suspended in DI water and the concentration was adjusted to 2.5×10^6 beads/mL for calibration of the device's performance.

E. coli DH5α strain was inoculated into a tryptic soy broth and cultured overnight in a 37°C incubator. *E. coli* cells were pelleted by centrifuging and then resuspended in PBS solution. The concentration of *E. coli* suspension was estimated by its optical density at 600 nm (OD600), which was previously calibrated by comparison of measured OD600 of a *E. coli* suspension and the concentration calculated from manual counting using a hemocytometer (Hausser Scientific, Horsham, PA, USA) under a microscope (Eclipse E200, Nikon, Mississauga, Canada). The calibration shows that an OD600 of 1 corresponds to a concentration of 8.3×10^8 cells/mL with an RSD of 8%.

Since water samples taken from environmental sources such as surface water or drinking water usually contain some inorganic particles, highly uniform blank polystyrene beads, 2 and 4 μm diameter (2.00 ± 0.04 and 4.20 ± 0.21 μm, respectively; Invitrogen, Burlington, Canada), were added into

the *E. coli* suspension to test their influence on the detection of *E. coli*. The concentrations of *E. coli*, 2 and 4 μm diameter beads in the mixture are 4.5×10^6 , 2.5×10^6, and 2.5×10^6 beads/mL, respectively.

The concentration of *E. coli* used in the experiments reported in this work is 10^6 cells/mL, which is much higher than the concentration of *E. coli* in drinking water or surface water, usually 0–100 cells/mL. Therefore, a preconcentration of the water sample should be performed to increase the concentration of *E. coli* by 3–6 orders of magnitude. However, the preconcentration stage is not included in this work.

2.4 Data collection and analysis

The sampling frequency used for data acquisition was 20 kHz. All data were collected and saved on a hard drive. The data were then analyzed using our custom-developed Matlab codes. Raw data of SSC light intensity collected in 1 s is shown in Fig. 2a as an example to illustrate the data analysis. Here, one short burst exceeding the threshold (a, inset) is considered to be one event where a bacterium or bead passes through the interrogation region. Figure 2b demonstrates the method to determine the threshold used to discriminate SSC light signals of events from the background noise. A higher threshold will ignore a portion of events, resulting in less total count of events. A lower one will add a portion of background noise into the total count of events, resulting in a large false count. Thus, a trade-off between maximum total count of events and minimum false count requires the threshold to be a minimum value with an acceptable false count. Since the majority of the data points is from background noise and its histogram is a Gaussian distribution (b, inset), the threshold is chosen to be four times of its SD, [21] which means a false count of 32 out of 1 million data points in a 50-s collection.

3 Results and discussion

3.1 Testing on beads

The performance of this microflow cytometer is first calibrated by testing with highly uniform polystyrene beads of diameter of 1 μm. Figure 2c shows 1-s raw data of SSC signals in a 50-s collection and the threshold for event detection, and Fig. 2d shows the statistical histogram of all events and its Gaussian fitting yielding a CV of 19.1% for testing on 1 μm beads by this microflow cytometer with beam size of 10 μm. This CV is relatively high compared to conventional flow cytometer because only 2D hydrodynamic sample centering is used. Since there is no vertical confinement of the beads in the microfluidic channel, then they may vary in the vertical direction, giving rise to a larger variation of SSC signal and hence a larger CV.

3.2 Counting *E. coli*

Fifty-second measurements were performed successively ten times to count *E. coli* suspension in PBS with a concentration of 7.3×10^6 cells/mL. The sample and sheath flow rates are fixed at 50 and 313 μL/h, respectively. The expected throughput of *E. coli* is the product of *E. coli* concentration and the sample flow rate, and is calculated to be 101.4 cells/s. Experimental throughputs of the *E. coli* and *S/N*s for each measurement are shown in Fig. 2f. The decreasing trend with time of the *E. coli* throughput arises from the decreasing effective *E. coli* concentration due to its precipitation in the sample syringe during these measurements. However, the average throughput is 92% of the expected value with an RSD of 9%. Also, S/Ns between 11 and 13 reduce the possibility of false counting from the background noise. The histograms of event signals in the first, fifth, and tenth measurements are shown in Fig. 2e, in which a wide population distribution can be found because the size of *E. coli* cells residing on different growth phases will vary. In addition, rod shape of *E. coli* cells results in a higher scattering cross-section than spherical particles when the cells pass through the interrogation area, causing a larger variation of SSC signal intensity.

Varying the sample flow rates from 50 to 150 μL/h with a fixed sheath flow rate of 313 μL/h was used to study the effect of the sample-to-sheath flow rate ratio on the detection efficiency of counting *E. coli*, as shown in Table 1. The sample stream width is calculated using the following equation,

$$ d = \frac{F R_{\text{sample}}}{1.5 \left(F R_{\text{sample}} + F R_{\text{sheath}} \right)} D, $$

where d is the focused sample stream width; FR_{sample} and FR_{sheath} are sample and sheath flow rates, respectively; D is width of microfluidic channel (50 μm for the device used). This equation is simplified from Eq. (11) in [33] with the assumption that the densities of sample and sheath solutions are equal. This assumption is reasonable because the difference in their relative density is less than 4×10^{-6}, which is calculated using parameters of *E. coli*, pellet density (1.06 g/mL), [34] cell volume (0.6–0.7 μm^3) [35] and concentration (4.9×10^6 cells/mL) used in the experiment.

From Table 1, a trade-off exists between the detection efficiency, the ratio of the measured throughput to the expected throughput, and the sample-to-sheath flow rate ratio. When the ratio is 0.16, the sample stream width is 4.6 μm, *E. coli* cells are confined to pass through the center of interrogation region and thus totally detected. However, when the sample stream width increases, the number of *E. coli* cells passing through the interrogation region near the edges also increases. SSC light from these cells has a higher possibility to exit the acceptance angle of the objective and is consequently missed for counting, resulting a reduced detection efficiency. This is in agreement with previously reported results in [16]. The *S/N*s between 9.7 and 11 ensure low possibility of false counting from the background noise.
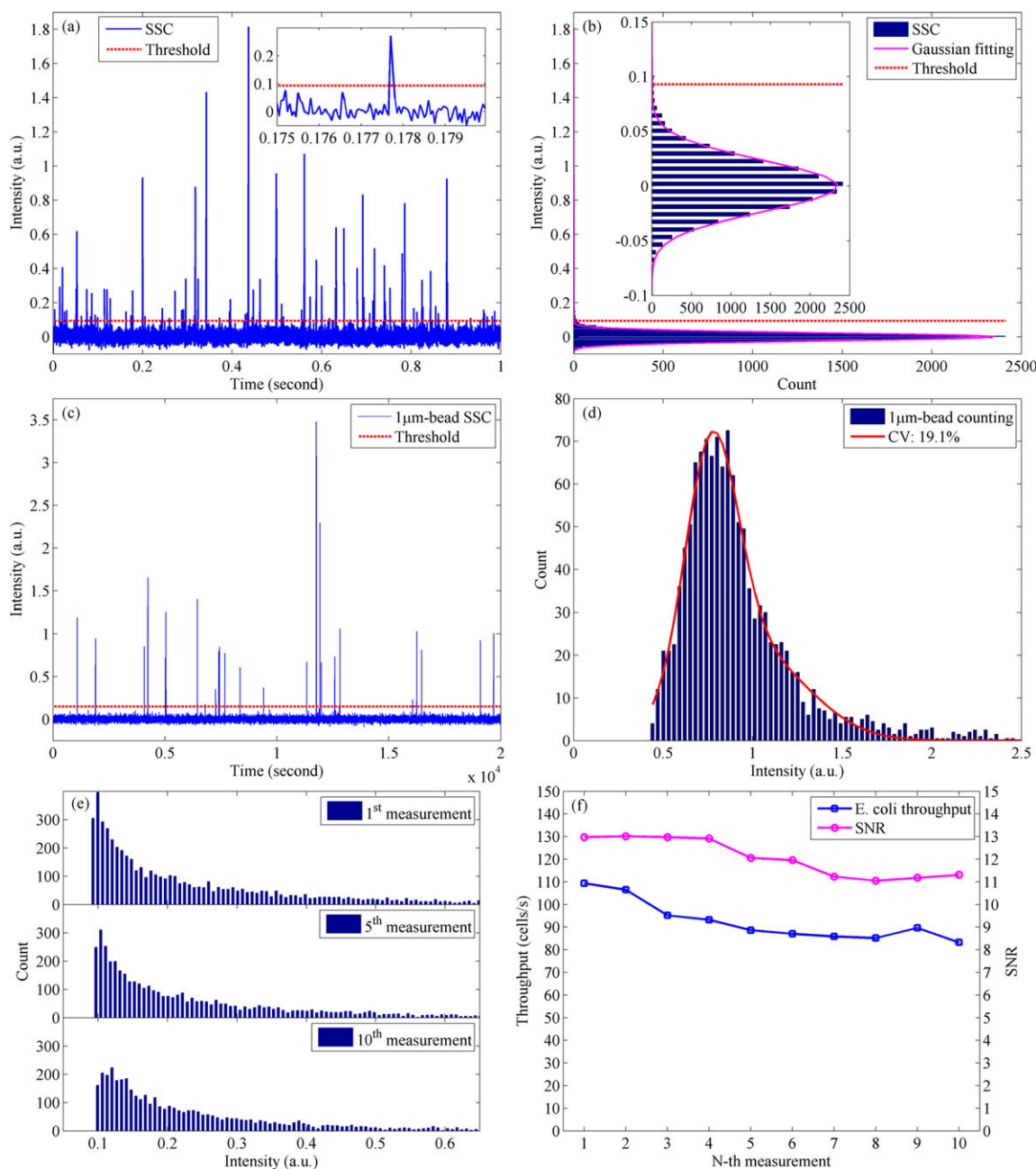
Figure 2. (a) One-second raw data of SSC light signals (solid) and the threshold (dashed) used to discriminate event signals from background noise; (a, inset) a detailed display of one event that SSC light signal bursts above threshold when a bacterium or bead passes through the interrogation region. (b) statistical histogram (bars) of all the raw data points in (a), its Gaussian fitting (solid) and determined threshold (dashed); (b, inset) a detailed view of background noise distribution; (c) One-second raw data of SSC signals (solid) from 1 μm diameter blank polystyrene beads in a 50-s collection and the determined threshold (dashed); (d) statistical histogram (bars) of all events detected and its Gaussian fitting (solid) used to calculate the CV of 19.1%; (e) statistical histograms of events in the first, fifth, and tenth measurements; (f) throughputs of *E. coli* counting (square) and SNRs (circle) for ten successive measurements with 50-s collection for each. The *E. coli* concentration is 7.3×10^6 cells/mL and the sample and sheath flow rates are 50 and 313 μL/hour, respectively.

3.3 Mixture of *E. coli* and beads

Interference of particles on counting *E. coli* is tested by adding 2 and 4 μm diameter polystyrene beads into the *E. coli* suspension samples. Ten measurements were performed to check the repeatability of the experiments and Fig. 3 shows results

of a typical experiment. Figure 3a displays 1-s SSC signal intensity with thresholds of *E. coli* and beads, 2 and 4 μm beads; (b1) shows the histogram of all events in the 50-s collection in logarithmic scale while (b2) and (b3) show the detailed histograms of *E. coli* and beads as well as their Gaussian fittings, respectively. The population distribution of *E. coli* is

Table 1. Effect of the sample-to-sheath flow rate ratio on sample stream width, *E. coli* throughputs, detection efficiency, and SNR

Sample flow rate (µL/h)	Sample-to-sheath flow rate ratio[a]	Sample stream width (µm)[b]	Measures throughput (cells/s)[c]	Expected throughput (cells/s)[d]	Detection efficiency (%)[e]	*S/N*
50	0.16	4.6	65.8 ± 4.9	68	97 ± 7	10.7
75	0.24	6.4	85.3 ± 2.6	102	84 ± 3	11.0
100	0.32	8.1	86.2 ± 1.9	136	63 ± 1	10.4
125	0.40	9.5	91.0 ± 5.9	170	13 ± 3	10.4
150	0.48	10.8	100.8 ± 7.7	204	45 ± 8	9.7

a) Sheath flow rate is fixed at 313 µL/h.
b) Calculated as described in text.
c) Obtained from eight successive measurements with 50-s collection for each.
d) Product of sample flow rate and sample concentration of 4.9×10^6 cells/mL.
e) Ratio of measured throughput to expected throughput.

clearly separated from that of 2 and 4 µm beads, indicating that the interference of 2 and 4 µm beads can be removed based on the different range of SSC signal intensity. The SSC signal intensity is positively correlated to the particle size and refractive index difference between the particles and water. And the refractive index of *E. coli* is very close to water because an *E. coli* cell is mostly composed of water. Therefore, interference from particles with sizes of 2 µm and larger can be eliminated based on the SSC signal intensity. However, interference from smaller particles exists, which requires other technique for differentiation, such as labeling *E. coli* with dye-conjugated antibody and collecting fluorescent and SSC signals simultaneously.

3.4 Comparison

In Table 2, a comparison between reported results and our work is provided. An important advantage of this work is achieving comparable detection efficiency with other works using a microflow cytometer of reduced system complexity. This was obtained by integrating the input waveguide and beam-shaping lens system on chip [36, 37] and utilizing simple 2D hydrodynamic sample centering that only requires

one channel of sheath flow. Integration of beam-shaping lens system eliminates the bulky lens system and accessories required to position the large lens system for optical path alignment, thus reducing the system cost.

4　Concluding remarks

Counting of *E. coli* in PBS is demonstrated by using a microflow cytometer based on a photonic–microfluidic integrated device. The integrated system consists of input waveguides, a beam-shaping lens system, and microfluidic channels with a 2D hydrodynamic focusing. Only the SSC light signals from samples are collected in free space and used for counting, allowing for detecting bacteria in water without tagging them. A detection efficiency of 92% is achieved at a throughput of 101 cells/s when compared with standard counts using a hemocytometer. The detection efficiency is correlated to the sample-to-sheath flow rate ratio. A high detection efficiency of 97% is achieved at a low ratio of 0.16. Tests on mixtures of *E. coli*, 2 and 4 µm diameter polystyrene beads show distinct separation on their scattering intensities, indicating that interference from particles of similar or larger sizes can be easily removed.
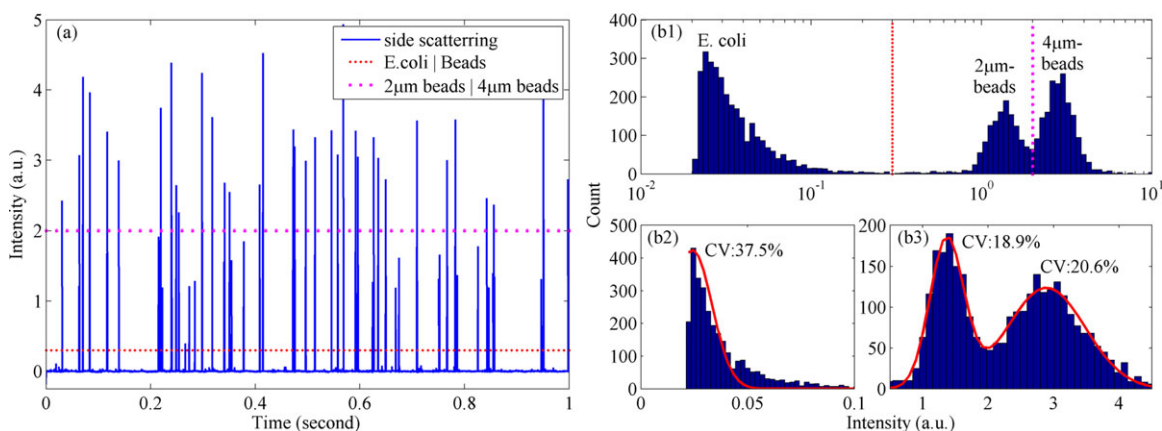

Figure 3. (a) One-second display of SSC signal intensity in a 50-s collection testing on a mixture of *E. coli*, 2 and 4 µm diameter beads (solid), intensity separations between *E. coli* and beads (dashed), between 2 and 4 µm diameter beads (dotted); (b1) statistical histograms of events produced by the mixture (bar) with logarithmic scale of intensity, (b2, b3) statistical histograms of events from *E. coli* and beads with linear scale of intensity and their Gaussian fittings, respectively.

Table 2. Summary of reported performances of similar microflow cytometers and from this work

Ref.	Sample	Sample centering technique	Excitation light beam shaping	Throughput (particles/s)	Detection efficiency (%)	
					Fluo.	SSC
[16]	0.93 µm beads	2D electrokinetic	3D free space	15	98	-
[22]	E. coli	2D electrokinetic	3D free space	36	94	-
[23]	1 µm beads	2D hydrodynamic	3D free space	416.7	91.3	88.9
[23]	E. coli	2D hydrodynamic	3D free space	350	89.7	94.5
[24]	1.9 µm beads	2D hydrodynamic	3D free space	17 000	97	-
This work	E. coli	2D hydrodynamic	2D on-chip	101	-	92

5 References

[1] Rompré, A., Servais, P., Baudart, J., de Roubin, M.-R., Laurent, P., *J. Microbiol. Methods* 2002, *49*, 31–54.

[2] Seidler, R. J., Evans, T. M., Kaufman, J. R., Warvick, C. E., LeChevalier, M. W., *J. Am. Water Works Assoc.* 1981, *73*, 538–542.

[3] Amann, R. I., Ludwig, W., Schleifer, K.-H., *Microbiol. Rev.* 1995, *59*, 143–169.

[4] Reynolds, K. A., Mena, K. D., Gerba, C. P., *Rev. Environ. Contam. Toxicol.* 2008, *192*, 117–158.

[5] Shinwari, M. W., Deen, M. J., Landheer, D., *Microelectron. Reliab.* 2007, *47*, 2025–2057.

[6] Seo, K. H., Brackett, R. E., Frank, J. F., *Int. J. Food Microbiol.* 1998, *44*, 115–123.

[7] Yamaguchi, N., Sasada, M., Yamanaka, M., Nasu, M., *Cytometry A* 2003, *54A*, 27–35.

[8] Clarke, R. G., Pinder, A. C., *J. Appl. Microbiol.* 1998, *84*, 577–584.

[9] Gunasekera, T. S., Attfield, P. V., Veal, D. A., *Appl. Environ. Microbiol.* 2000, *66*, 1228–1232.

[10] Hoefel, D., Grooby, W. L., Monis, P. T., Andrews, S., Saint, C. P., *J. Microbiol. Methods* 2003, *55*, 585–597.

[11] Lepeuple, A. S., Gilouppe, S., Pierlot, E., de Roubin, M. R., *Int. J. Food Microbiol.* 2004, *92*, 327–332.

[12] Hammes, F., Berney, M., Wang, Y., Vital, M., Koster, O., Egli, T., *Water Res.* 2008, *42*, 269–277.

[13] Berney, M., Hammes, F., Bosshard, F., Weilenmann, H.-U., Egli, T., *Appl. Environ. Microbiol.* 2007, *73*, 3283–3290.

[14] Steen, H. B., Boye, E., *Cytometry* 1980, *1*, 32–36.

[15] Sims, C. E., Allbritton, N. L., *Lab Chip* 2007, *7*, 423–440.

[16] Schrum, D. P., Culbertson, C. T., Jacobson, S. C., Ramsey, J. M., *Anal. Chem.* 1999, *71*, 4173–4177.

[17] Deen, M. J., Basu, P. K., *Silicon Photonics: Fundamentals and Devices*, Wiley, Chichester, UK; Hoboken, NJ., 2012.

[18] Mogensen, K. B., El-Ali, J., Wolff, A., Kutter, J. P., *Appl. Opt.* 2003, *42*, 4072–4079.

[19] Hsiung, S.-K., Lee, C.-H., Lee, G.-B., *Electrophoresis* 2008, *29*, 1866–1873.

[20] Rosenauer, M., Vellekoop, M. J., *Biomicrofluidics* 2010, *4*, 043005.

[21] Kennedy, M. J., Stelick, S. J., Sayam, L. G., Yen, A., Erickson, D., Batt, C. A., *Lab Chip* 2011, *11*, 1138–1143.

[22] McClain, M. A., Culbertson, C. T., Jacobson, S. C., Ramsey, J. M., *Anal. Chem.* 2001, *73*, 5334–5338.

[23] Mu, C., Zhang, F., Zhang, Z., Lin, M., Cao, X., *Sens. Actuators B Chem.* 2011, *151*, 402–409.

[24] Simonnet, C., Groisman, A., *Anal. Chem.* 2006, *78*, 5653–5663.

[25] Watts, B. R., Zhang, Z., Xu, C.-Q., Cao, X., Lin, M., *Biomed. Opt. Express* 2012, *3*, 2784–2793.

[26] Watts, B. R., Zhang, Z., Xu, C. Q., Cao, X., Lin, M., *Electrophoresis* 2012, *33*, 3236–3244.

[27] Watts, B. R., Kowpak, T., Zhang, Z., Xu, C.-Q., Zhu, S., Cao, X., Lin, M., *Micromachines* 2012, *3*, 62–77.

[28] Watts, B. R., Zhang, Z., Xu, C. Q., Cao, X., Lin, M., *Electrophoresis* 2014, *35*, 271–281.

[29] Kowpak, T., Watts, B. R., Zhang, Z., Zhu, S., Xu, C., *Macromol. Mater. Eng.* 2010, *295*, 559–565.

[30] Watts, B. R., Kowpak, T., Zhang, Z., Xu, C., Zhu, S., *Biomed. Opt. Express* 2010, *1*, 848–860.

[31] Zhang, Z., Zhao, P., Xiao, G., Watts, B. R., Xu, C., *Biomicrofluidics* 2011, *5*, 046503.

[32] Watts, B.R., Zhang, Z., Xu, C., Cao, X., Lin, M., *Biomed. Opt. Exp.* 2013, *4*, 1051–1060.

[33] Lee, G.-B., Hung, C.-I., Huang, G.-R., Hwei, B.-H., Ke, B.-J., Lai, H.-F., *J. Fluids Eng.* 2001, *123*, 672–679.

[34] Schultz, S. G., Epstein, W., Solomon, A. K., *J. Gen. Physiol.* 1963, *47*, 329–346.

[35] Kubitschek, H. E., *J. Bacteriol.* 1990, *172*, 94–101.

[36] Howlader, M. M. R., Selvaganapathy, P. R., Deen, M. J., Suga, T., *IEEE J. Sel. Top. Quantum. Electron.* 2011, *17*, 689–703.

[37] Qinm, Y., Howlader, M. M. R., Deen, M. J., Haddara, Y., Selvaganapathy, P. R., *Sens. Actuators B Chem.* 2014, *202*, 758–778.